TNO-Defensieonderzoek

TNO-report
PML 1994-A33

September 1994

Copy no:- 81

General description of the Missile Systems Damage Assessment Code (MISDAC)

TDCK RAPPORTENCENTRALE
Frederikkazerne, gebouw 140
v/d Burchlaan 31 MPC 16A
TEL. : 070-3166394/6395
FAX. : (31) 070-3166202
Postbus 90701
2509 LS Den Haag

TNO Prins Maurits Laboratory

TNO Defence Research

TD 94-0474
P.O Box 45
2280 AA Rijswijk
The Netherlands

Fax +31 15 84 39 91
Telephone +31 15 84 28 42

TNO-report
PML 1994-A33

September 1994
Copy no:- 8

General description of the Missile Systems Damage Assessment Code (MISDAC)

Author:

W. Haverdings

DO-assignment no.:
A92/KM/407

Number of copies:
28
Number of pages:
(excl. distr. list and RDP)
43

Netherlands organization for applied scientific research

TNO Defence Research consists of:
the TNO Physics and Electronics Laboratory,
the TNO Prins Maurits Laboratory and the
TNO Institute for Perception.

MANAGMENTUITTREKSEL

Titel	:	General description of the Missile Systems Damage Assessment Code (MISDAC)
Auteur	:	W. Haverdings
Datum	:	september 1994
Rapportnummer	:	PML 1994-A33
DO-opdrachtnr.	:	A92/KM/407

In het kader van de opdracht A92/KM/407 "Kwetsbaarheid van anti-schip geleide wapens" is een code ontwikkeld welke een analyse beoogt te kunnen geven van het gedrag van een inkomend geleid wapen dat wordt bestreden door verdedigingsmiddelen van het schip (of vloot) dat wordt aangevallen. Met deze code kunnen de schadelijke gevolgen van een exploderende warhead op een inkomend anti-schip geleid wapen worden bepaald. In het rapport wordt een algemene beschrijving gegeven van de Missile Systems Damage Assessment Code (MISDAC), die ontwikkeld werd uit een tweetal bestaande codes namelijk Target Vulnerability Assessment Code (TARVAC) en Missile Vulnerability Assessment Code (MISVAC).
De code berekent voor iedere onderschepping welke onderdelen van het geleide wapen worden beschadigd, waarbij rekening wordt gehouden met de onderscheppingsgeometrie, de relatieve snelheden, de verschervende werking van de warhead, en de penetratie van de scherven in het doel. De locatie van de springpunten in de buurt van het doel kan enerzijds worden bepaald met behulp van speciale programmatuur, of anderzijds via geleverde springpunten. Ook is het mogelijk de schade door projectielen te bepalen, bijvoorbeeld afkomstig van snelvuur kanonnen (Goalkeeper).
De reden voor de ontwikkeling van MISDAC is het verkrijgen van een beter inzicht in de beschadigingen die kunnen ontstaan in het doel, eventueel gespecificeerd naar type onderdeel, omdat in de voormalige code MISVAC, die tijdens de NATO Anti-Air Warfare System (NAAWS) periode werd ontwikkeld, slechts grotere delen van het doel (resp. secties of sectoren) konden worden geanalyseerd. Hierdoor is MISVAC beperkt tot de drie in NAAWS gedefinieerde doelen vanwege de door de Britten ingebrachte "experimentele" gegevens. De feitelijke achtergronden zijn onduidelijk en maken van dit model dan ook een "black box" benadering.
Ten opzichte van de langer bestaande code TARVAC bestaat nu de mogelijkheid om schade ten gevolge van directe treffers op afzonderlijke componenten nader te analyseren, alsmede de schade door blast. Laatstgenoemde mogelijkheid is echter op eenvoudige wijze geïmplementeerd, omdat een dynamische berekening van constructies niet in een schootslijnmethode kan worden uitgevoerd.
Nadat de schade berekeningen zijn uitgevoerd wordt door een andere code Flight Path Simulation of Missiles (FLIPSIM) bepaald of het beschadigde missile in staat is het schip alsnog te treffen, gegeven de interceptie afstand (ook wel beschadigingsafstand genoemd) en het type manoeuvre dat wordt uitgevoerd. De totale uitkomst van de berekeningen geeft de uitschakelkans van het missile, gegeven een (succesvolle) onderschepping. Tevens bestaat de mogelijkheid om op basis van het gedrag van het beschadigde missile te komen tot bepaalde klassen van (verstoorde) banen, hetgeen een hulpmiddel kan zijn voor de zogenaamde "kill assessment" studies.

In het rapport wordt ingegaan op vele details met betrekking tot de schootslijn benadering, de implementatie van blast effecten en de wijze waarop de diverse uitschakel mogelijkheden worden verwerkt.
Het rapport concludeert met het feit dat MISDAC is ontstaan uit de twee oudere codes, namelijk de "standaard" code TARVAC en de daaruit afgeleide code MISVAC. Hierbij zijn van beide codes de nadelen zoveel mogelijk vermeden, en de voordelen benut.
De uiteindelijke kans op uitschakeling van het missile moet nog worden geïmplementeerd via geavanceerde zogenaamde 6-DOF simulaties met behulp van FLIPSIM. De koppeling van FLIPSIM aan MISDAC is een aspect dat in het vervolgonderzoek plaats zal vinden.

CONTENTS

LIST OF SYMBOLS

A_{min}	-	minimum presented area
A_{max}	-	maximum presented area
$\bar{A}_p$, A_p	-	(average) presented area
A_w	-	wetted surface
A, B, C		Westine constants
a, b, c	-	constants
c	-	wave speed
c_a	-	speed of sound (air)
C_D	-	drag coefficient
d	-	line-of-sight distance
d_{max}	-	max. penetration distance
D	-	(projectile) diameter
L	-	length
m	-	projectile/fragment mass
M	-	Mach number: $M=V/c_a$
M_o	-	molecular weight
P_k	-	probability of kill
P_{dh}	-	probability of damage given a hit
P_{kd}	-	probability of kill given damage
P_{kh_c}	-	probability of kill given a hit on a component
p	-	pressure
p_s	-	peak (side-on) overpressure
R	-	range between missile and target
R_a	-	absolute gas constant
R_{hit}	-	range when hit by blast
R_i	-	initial range (intercept)
R_c	-	charge radius (TNT)
R_{crit}	-	critical range for blast damage
r	-	radius
$\bar{S}_n$, S_n	-	(average) shape number
t	-	time ; thickness
t_{max}	-	max. plate thickness
t_p	-	positive phase duration
Δt	-	difference in time-of-arrival
T	-	temperature
u	-	flow (particle) velocity
$\bar{U}$, U_s	-	(average) shock wave velocity
V	-	velocity
V_f	-	fragment velocity
V_{fa}	-	average initial fragment ejection velocity

V_{fo}	-	initial fragment ejection velocity
V_{fi}	-	impact fragment velocity
V_{fmt}	-	relative fragment-target velocity
V_{fta}	-	average relative fragment-target velocity
V_{fto}	-	initial relative fragment-target velocity
V_{fti}	-	impact relative fragment-target velocity
V_m	-	missile velocity
V_p	-	projectile velocity
V_{pt}	-	relative projectile-target velocity
V_t	-	target velocity
V_r	-	residual velocity
w	-	width
W	-	warhead mass, TNT-eq.
x,y	-	co-ordinates; variables
Z	-	scaled range $Z=R/W^{1/3}$

Greek symbols

α	-	azimuth angle
ψ	-	elevation angle
$\varepsilon, \varepsilon_{x,y}$	-	dispersion angles
φ	-	miss orientation angle; angle of incidence
β	-	pitch angle; Weibull parameter; time factor
χ	-	fragment ejection angle
γ	-	yaw angle,; ratio of specific heats, $\gamma=1.4$
θ	-	fragment normal impact angle
ξ	-	slope parameter
Ω	-	random (0,1) variable
ρ, ρ_m	-	density (of fragment)
ρ_a	-	air density (sea level)
ω	-	fragment rotation speed

List of abbreviations

AAM	Air-to-Air Missile
AMD	Miss Distance orientation angle
ASM	Anti-Ship Missile
ASSM	Anti-Surface-Ship Missile[1]
CPA	Closest Point of Approach
FLIPSIM	Flight Path Simulation of Missiles
MD	Miss Distance
MISDAC	Missile Systems Damage Assessment Code

1 Obsolete expression to indicate an ASM but not to be confused with Air-to-Surface. Air-to-Surface is designated as Air-to-Ground (AGM) for land-based missiles and as Anti-Ship for naval versions.

MISDAC	Missile Systems Damage Assessment Code
MISVAC	Missile Vulnerability Assessment Code
MRP	Missile Reference Point, (the geometric centre of the missile)
NAAWS	NATO Anti Air Warfare System
SBS	Subsonic sea skimming missile
SHD	Supersonic high diving missile
SSS	Supersonic sea skimming missile
SEAROADS	Simulation, Evaluation, Analysis on Research of Air Defence Systems
SHAMDAT	Sectional Hardness Methodology for Damaged Air Targets
TARVAC	Target Vulnerability Assessment Code
TGT	Target
TNT	Tri-Nitro-Tolueen (or Trotyl), a chemical high-explosive compound
TRP	Target Reference Point (the geometric centre of the target)
WHD	Warhead (centre)

1 INTRODUCTION

This report has been written to assist the Royal Netherlands Navy in developing adequate means to defend their battleships against future threats, particularly from incoming antiship missiles. In addition to research being conducted on survivability enhancement of battleships, the Directorate of the Royal Navy Materiel (DMKM) required an investigation into the effectiveness of the air defence systems currently installed, and to be installed on board future battleships, within the framework of A92/KM/407, "Vulnerability Analysis of Anti-Surface-Ship-Missiles". This report, however, only deals with the methodology that has been developed to assess the vulnerability of missile targets.

In the Weapon Effectiveness research group of the Weapons & Platforms Division at the TNO-Prins Maurits Laboratory (PML), a target vulnerability assessment code (TARVAC) has been developed. This code assesses the effects of projectiles and/or fragments with respect to the capability of killing a target. Basically, the method employs a shot line technique, which represents the trajectory of an actual projectile or fragment. Several parts of the code deal with geometrical intersections of such shot lines with the target. In the code, the target is represented by a computerised description, where components are represented by solids (geometrical figures), to which certain material properties (e.g. material density, dimensions) are assigned.

When dealing with fast incoming antiship missiles the defensive capabilities on board the ship are tested to the limits. The missile must be engaged far enough away to prevent the missile or its debris from hitting the ship. If any part of the missile hits the ship, it may still inflict severe damage on the ship. Apart from a fast reacting air defence asset, the kill of the missile must be ensured. To this end all damaging effects having a certain kill capability are addressed into more detail, not only fragment impacts, but also direct hits (from a surface-to-air missile) and blast damage leading to structural kill. In this respect it was found that TARVAC was inadequate, and hence an improvement was necessary.

The direct hit option is dealt with by including so-called missile representing points, and regarding relative missile-target trajectories as equivalent shot lines. The blast damage option, however, cannot be dealt with using a shot line approach. Although several options exist to model blast damage, it was decided to keep the level of detail for blast modelling as simple as possible. To this end, so-called blast-critical components were introduced in addition to specified damage radius criteria. Complex blast wave - target interactions are then ruled out by definition, but it is emphasised that fragment damage predominates the overall damage to the target.

Therefore a new code has been developed which in comparison with the former code is named Missile Systems Damage Assessment Code (MISDAC). MISDAC is a further development of the Missile Vulnerability Assessment Code (MISVAC), which was derived from TARVAC and the code SHAMDAT (Sectional Hardness Methodology for Damaged Air Targets) from the UK [1]. MISVAC has been used exclusively in the NATO Anti-Air Warfare System (NAAWS) evaluation, and has been applied in the SEAROADS project to assess the lethality of the NATO Sea Sparrow missile warhead [2]. Although MISVAC includes the options mentioned before, it lacks the detailed analysis of internal components being damaged, while the overall kill assessment includes the target-range-to-go as a simple factor. Target-range-to-go is defined as the range from the ship being attacked, at which damage to the target occurs, also called the intercept range. Although by far one of the fastest computational methods, much of the background is

seemingly based on experimental data and/or educated guesses making the whole concept a black-box like approach. MISDAC is constructed in such a way that detailed damage assessment of components is performed - similar to TARVAC - and that post-damage flight trajectories, given damage to the missile systems, are conducted by a code called Flight Path Simulation of Missiles (FLIPSIM) to find the ultimate probability whether the missile or its debris will hit the ship, which is a measure of the probability of missile kill. In other words, the output of MISDAC serves as input for FLIPSIM. Figure 1 illustrates the development of MISDAC showing the essential modules embedded in the program.

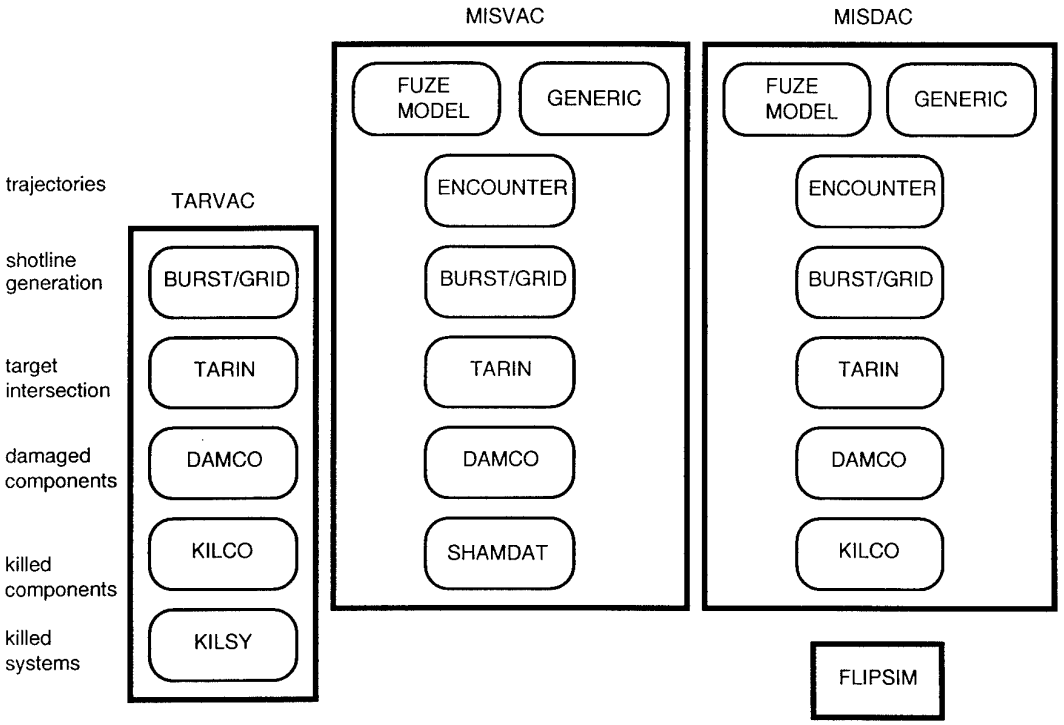

Figure 1 Schematic development of MISDAC

In the BURST/GRID module, the shotlines from a detonating warhead are generated and the fragments hitting the target perimeter[1] are determined. In the TARIN module, a more accurate determination is performed in which components of the target are intersected. In DAMCO, all components are determined that are penetrated using ballistic penetration relationships. In KILCO, the probability of kill of the damaged components are determined using kill criteria, and finally in KILSY, the probability of kill of all systems making up the complete target are determined using special logical combinations according to a kill tree. In MISVAC, the KILCO module has been replaced by the British SHAMDAT module, while DAMCO has been stripped because penetrations are not calculated. An extra feature in MISVAC (and also MISDAC) is the possibility to use a fuse model or a generic model to create burst points. However, at present the

1 The whole target is enclosed in a box.

fuse model only wo1ks for the three existing NAAWS targets (i.e. SBS, SSS and SHD missiles) for each of which a so-called stick-cone target model exists.
The computations in FLIPSIM are performed using dynamic flight trajectory simulations, where the missile aerodynamics and controls are incorporated in a six-degrees-of-freedom (6-DOF) simulation model. So, an assessment has to be performed about the residual missile's control and aerodynamics properties after being engaged, which forms the most difficult part of the study. The final outcome of the computations, i.e. the probability of kill of the missile given an engagement (either by guns or missiles) is then found using a logical combination of MISDAC with FLIPSIM. This report will describe the basic features of only the first part, i.e. MISDAC.

2 DESCRIPTION OF THE METHOD

Basically, the method employed in MISDAC is quite similar to the original method TARVAC [3]. This method has been developed over many years, and changes have been incorporated ever since. In principle, the target is geometrically represented by seven solids, viz.: box, pentahydron (5-planes), cylinder, (truncated) cone, parallelepiped, triangular plate (with thickness) and sphere. To model a component, several solids can be used, in addition to "negative" solids, by which voids etc. can be modelled. In the target database, the components are indicated by two 6-digit numbers which have a special meaning. The first 6 digits indicate the component number, which may be arbitrarily chosen. The second 6-digit number contains the component's physical information. The first digit must be either a 0, 1 or 2, indicating its vulnerability (0=non-vulnerable, 1=vulnerable to fragments, 2=vulnerable to blast). The next 2 digits represent the material code (ranging from 1 to 25) and the last 3 digits represent the void ratio in percentage (varying from 0 to 100 per cent).
One of the differences between MISDAC and TARVAC lies in the vulnerability code for a component being vulnerable to blast (=2). In essence, a blast-vulnerable component is represented by a cylinder with zero radius (or line element), so that its structure fits well in the standard target construction method using (the same) solids. However, shotline intersections with the actual component are omitted since the vulnerability code (=2) is tagged to skip this kind of operation.
In the missile-target engagement, where an incoming sea skimming missile target is intercepted by a surface-to-air missile (SAM) defending the ship, the engagement geometry is outlined in Figure 2. The main parameters driving the engagement are:

- missile velocity V_m
- target velocity V_t

  } which defines the relative missile-target velocity V_{mt}
- azimuth angle α
- elevation angle ψ
- miss distance MD
- miss distance orientation φ

The missile has a pitch (β) and yaw angle (γ) relative to its flight path. Due to symmetry the roll angle is ignored.

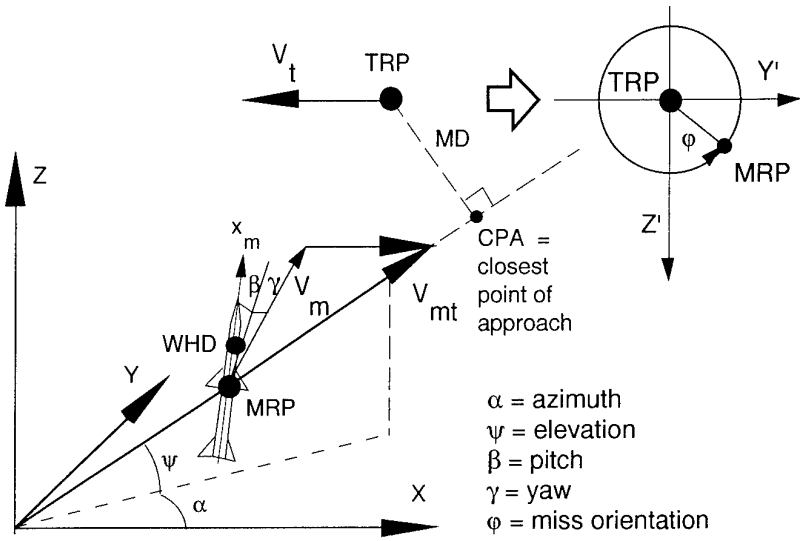

Figure 2 *Missile-target engagement geometry*

To maintain similarity with TARVAC, the target modelling uses the same co-ordinate system, but the target velocity is directed to the -x axis (left). The target and SAM missile are represented by their reference points TRP and MRP, which are located exactly in the geometric centres of the target and missile, respectively. Further explanation of the intercept geometry can be found in [1]. For each engagement, a set of relative missile-target trajectories is created defined by a (fixed) miss distance MD and a number of miss distance orientation angles (φ). In this way a number of parallel trajectories are created lying upon the cylinder around the target with the miss distance MD as its radius. Along each of the trajectories, a number of detonation points are selected, for example spaced at constant time intervals before and after t=0[1]. The point t=0 is exactly the point where the distance between missile and target is equal to the miss distance. This point is usually referenced as Closest Point of Approach (CPA), see Figure 3.

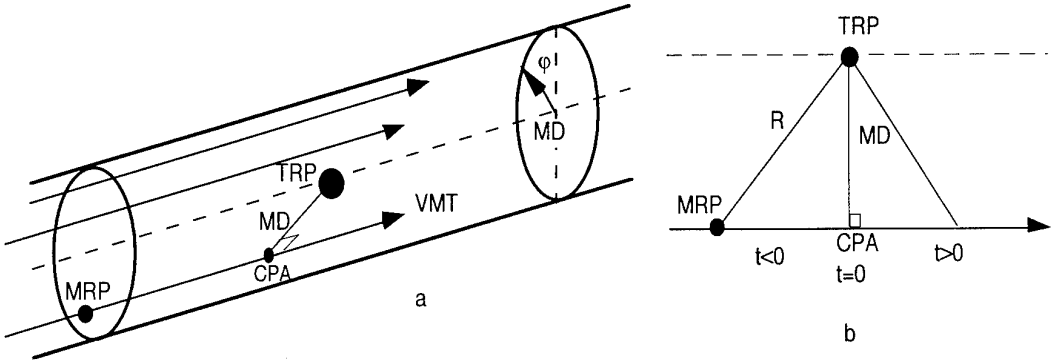

Figure 3 *Shot lines - missile target encounter*
a) - general view b) - 2-D view

1 Or one single fuse-determined burst point.

The results of the computations are then averaged over all burst points to give an average P_k for this miss distance. This generated encounter file, containing the possible detonation positions of the warhead relative to the target, can also be used in other external programs to estimate the actual fuse-triggered detonation points. In fact, this has been employed in earlier computations for the Royal Netherlands Navy project SEAROADS [2]. However, data pertaining to warhead burst points driven by proximity fuses are generally obtained from the TNO Physics and Electronics Laboratory.

3 PROJECTILE/WARHEAD DAMAGE EFFECTS

3.1 Shot line generation

To analyse the effects of projectiles hitting the target, or the effects of a warhead detonation in the vicinity of the target, the shot line technique is used. Each projectile or fragment trajectory is simulated by its corresponding shot line, having an identification number, a specified mass, velocity, origin and direction. A few options exist by which a grid of shot lines can be created. One option is to use a parallel grid of equally-spaced shot lines, "fired" from a certain direction to the target. For statistical purposes, a random position within a grid cell may be chosen. In the projected plane, the shot line co-ordinates are given by:

$$\left.\begin{aligned} x &= x_n + \Omega(x_{n+1} - x_n) \\ y &= y_m + \Omega(y_{m+1} - y_m) \end{aligned}\right\} \qquad (1)$$

where Ω is either fixed (Ω=0.5) or a (0,1) random variable in an (n,m) grid, see Figure 4.

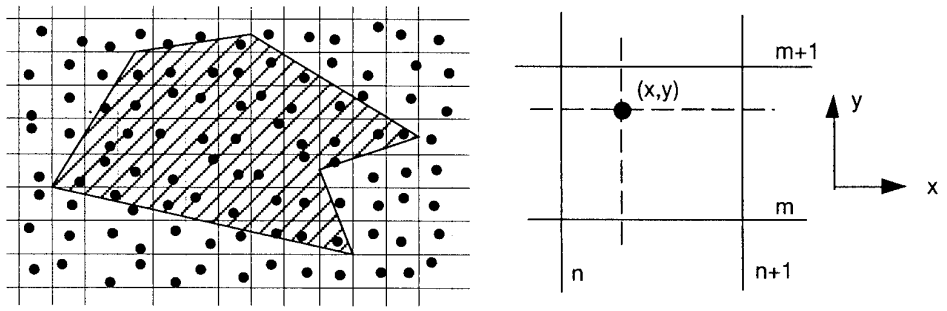

Figure 4 Rectangular grid with random shot lines

In another option, a so-called "aiming" grid can be selected, which is composed of an aiming point and a number of shot lines "fired" at this aiming point using a statistical error, usually a circular error normally distributed around the aiming point, see Figure 5. In the projected plane the shot line co-ordinates are found using bivariate normal deviates according to Box-Muller [4]:

$$\left.\begin{aligned} x &= \left[-2\ln\Omega_1\right]^{1/2}\cos(2\pi\Omega_2) \\ y &= \left[-2\ln\Omega_1\right]^{1/2}\sin(2\pi\Omega_2) \end{aligned}\right\} \qquad (2)$$

where Ω_1, Ω_2 are independent (0,1) random variables. The (x,y) deviates given a range R and an angular error ε yield the normal "hit"-distribution around the "aiming" point (0,0):

$$\left.\begin{aligned} x &= R\varepsilon_x\ \left[-2\ln\Omega_1\right]^{1/2}\cos(2\pi\Omega_2) \\ y &= R\varepsilon_y\ \left[-2\ln\Omega_1\right]^{1/2}\sin(2\pi\Omega_2) \end{aligned}\right\} \qquad (3)$$

where ε_x and ε_y are two independent errors. If they are equal, a circular error results. An example for R=1000 m, $\varepsilon_x=\varepsilon_y=$ 1 mrad is given in Figure 5.

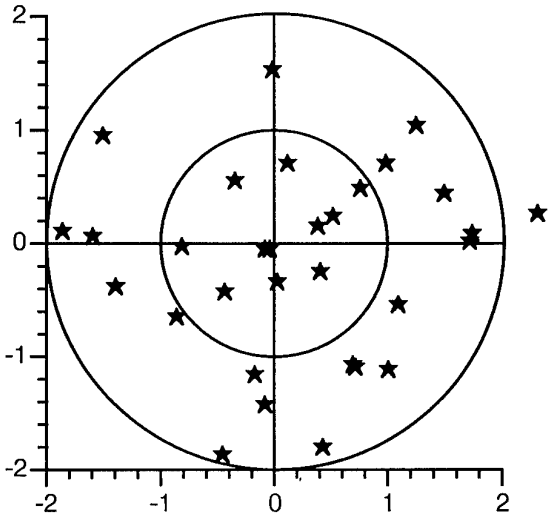

Figure 5 *Aimpoint and dispersion generated shot lines; R=1000 m, ε=0.001 rad*

This kind of approach enables the simulation of gun fire engagements, e.g. a Goalkeeper gun system defending a ship against a sea skimming missile.
The frequently used option is a grid of shot lines simulating the detonation of a warhead, which is assumed to generate numerous fragments emanating from the centre of the warhead.
Also the possible direct hit of the intercepting missile with the target is included. To this end the user must specify several missile representing points, which are being assumed to generate "direct-hit" shot lines, see Figure 6.

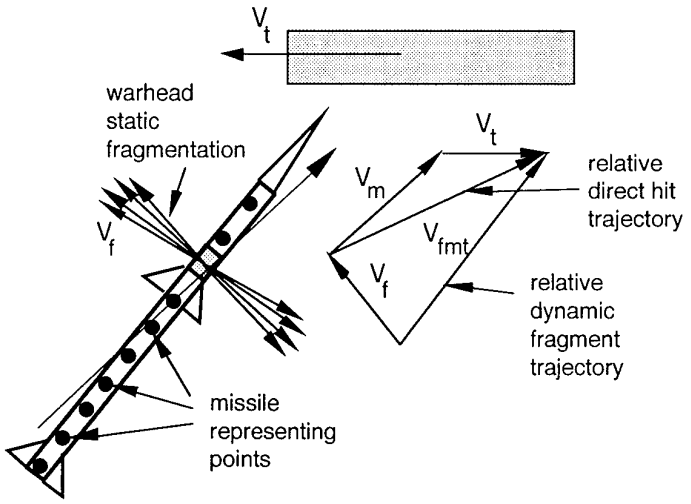

Figure 6 Warhead detonation and direct hit shot line simulation

This kind of engagement is typical of an air defence missile, e.g. Sea Sparrow, defending a ship against an incoming sea skimming missile.

3.2 Projectile trajectories

When considering shot lines simulating projectile trajectories, the target velocity may have a serious effect on the impact condition. In general, it is assumed that a projectile follows its (ballistic) flight to the target without motion around its flight path, i.e. yaw and spin are ignored. However, at impact on the target, flying with velocity V_t, the penetration process is changed significantly due to the velocity vector of the target relative to the projectile velocity vector, see Figure 7.

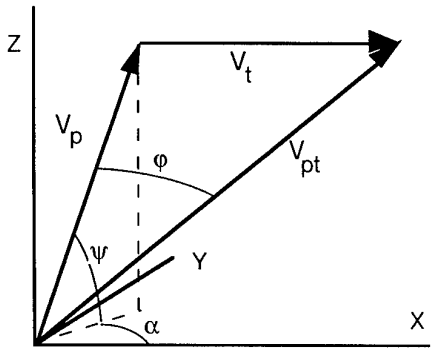

Figure 7 Influence of target velocity

Given the initial conditions of flight, i.e. azimuth (α) and elevation (ψ) angles, the original projectile velocity V_p is changed into the relative velocity V_{pt} by:

$$\underline{V}_{pt} = \underline{V}_p + \underline{V}_t \tag{4}$$

The projectile now exhibits an angle of incidence to the relative flight path, indicated by the dynamic angle of incidence φ, given as:

$$\cos\varphi = \frac{\left(\underline{V}_{pt} \bullet \underline{V}_p\right)}{\left|\underline{V}_{pt}\right|\left|\underline{V}_p\right|} \tag{5}$$

In a first approximation, the shape r(x) of the projectile is assumed to be parabolic (insert in Figure 8), i.e.:

$$r(x)=\frac{D}{2}\sqrt{\frac{x}{L}} \quad \text{hence:} \quad A_{max}=\int_0^L 2r(x)dx \qquad \text{(maximum presented area)}$$

where r(x) is the local projectile radius, D the maximum diameter and L the projectile length. The maximum presented area (A_{max}) is then found as: $A_{max} = \frac{2}{3}LD$ (viewed from the side), whereas the minimum presented area is: $A_{min}=\frac{\pi}{4} D^2$ (viewed from the front). The ratio between A and A_{min} is then approximated by:

$$\frac{A}{A_{min}} \approx \cos\varphi + \frac{8}{3\pi}\frac{L}{D}\sin\varphi \tag{6}$$

When dealing with fast flying aircraft or missiles and high-velocity projectiles, the dynamic angle of incidence (φ) may become as large as 20°, see Figure 8.

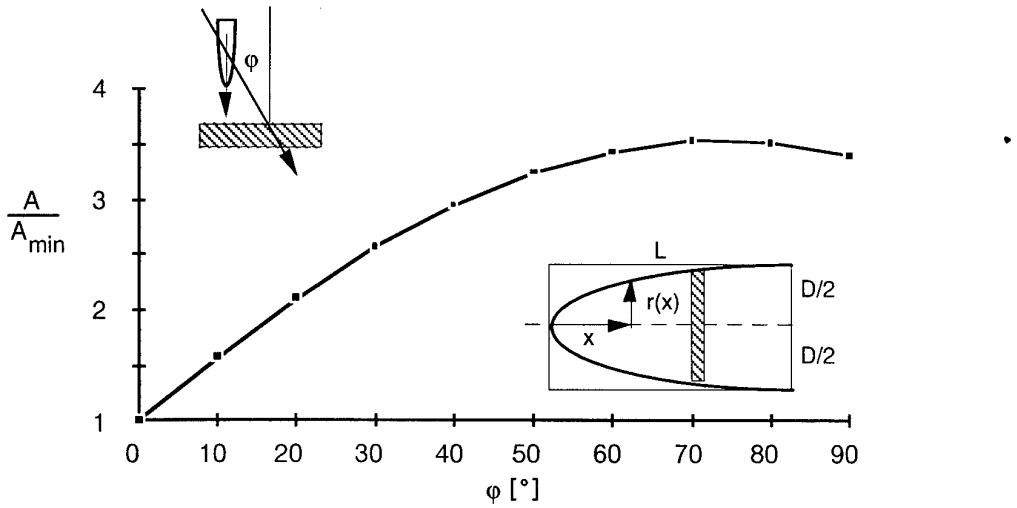

Figure 8 Influence of dynamic impact angle on the presented area of a projectile

Hence, instead of a circular hole, the projectile will create an oblong perforation that significantly reduces its penetration capability.

3.3 Fragment trajectories

The basic shot line data, such as mass, velocity and shape of the fragments are usually obtained from experiments. Given the warhead velocity vector $\underline{V}_m$, fragment (static) velocity vector $\underline{V}_f$ and target velocity vector $\underline{V}_t$, the relative velocity vector of the fragment when hitting the target, supposing that air drag is not incorporated, is equal to:

$$\underline{V}_{fmt} = \underline{V}_f + \underline{V}_m + \underline{V}_t \tag{7}$$

Hence, the fragments will strike the target with relatively high velocities, and may have an arbitrary orientation at impact due to tumbling.

3.4 Influence of air drag

To account for proper aerodynamic drag during its flight towards the target, each fragment is assumed to have a specific *average* shape, expressed by its non-dimensional average shape number [5], [6], [7]:

$$\bar{S}_n = \frac{\bar{A}_p}{Vol^{2/3}} \tag{8}$$

where $\bar{A}_p$ is the average presented area and Vol. is the volume of the fragment.
Dehn [6] gives an expression for the average presented area as:

$$\bar{A}_p = \frac{1}{4} A_w \tag{9}$$

where A_w is the wetted surface.
For a number of shapes, the average shape number can be found as:

$$\text{for a sphere:} \quad \bar{S}_n = \frac{\pi}{\left[\frac{4}{3}\pi\right]^{2/3}} = 1.21 \quad \text{(independent of size)} \tag{10}$$

$$\text{for a beam:} \quad \bar{S}_n = \tfrac{1}{2}(ab)^{1/3}\left[1 + \frac{1}{a} + \frac{1}{b}\right] \tag{11}$$

where a = L/t, b=w/t, for a beam with dimensions Lxwxt (L≥w≥t).
For a cube, where all dimensions are equal, it yields:

$$\bar{S}_n = 1.5 \text{ (independent of size)} \tag{12}$$

For a cylinder, it can be shown that:

$$\bar{S}_n = \left(\frac{1}{4}\pi a\right)^{1/3}\left[1 + \frac{1}{2a}\right] \tag{13}$$

where a = L/D of the cylinder.

When air drag must be incorporated, the absolute velocity of the fragment (i.e. $\underline{V}_m+\underline{V}_f$) must be used to determine certain air drag parameters, e.g. drag coefficient, dynamic pressure etc. Suppose the range to the target is R, and the initial absolute fragment velocity is $\underline{V}_{fo}$. The initial relative velocity to the target is then (Figure 9):

$$\underline{V}_{fto} = \underline{V}_{fo} + \underline{V}_t \tag{14}$$

If the fragment is retarded by air drag, the velocity at a range R from the origin can be estimated for small velocity changes, hence a constant drag coefficient, as [7]:

$$\underline{V}_{fi} = \underline{V}_{fo}F(R) \tag{15}$$

or, when applied to the relative fragment-target velocity:

$$\underline{V}_{fti} = \underline{V}_{fto}.F(R) + \underline{V}_t[1 - F(R)] \tag{16}$$

where the correction term F(R) has been derived in [7] as:

$$F(R) = \exp\left[-C_D \frac{1}{2}\rho_a \frac{\overline{A}_p}{m} R\right] \tag{17}$$

where ρ_a is the density of air, m is the fragment mass and C_D is the drag coefficient. The effect of burst altitude is included by virtue of changes in air density. From these velocities, the average velocity (i.e. harmonic mean) can be derived:

$$\underline{V}_{fta} = \frac{2}{\frac{1}{\underline{V}_{fto}} + \frac{1}{\underline{V}_{fti}}} = \underline{V}_{fa} + \underline{V}_t \tag{18}$$

where $\underline{V}_{fa}$ is the average relative fragment ejection velocity vector (Figure 9).
The difference in time-of-arrival can be approximated as:

$$\Delta t = \left[\frac{R}{\underline{V}_{fta}} - \frac{R}{\underline{V}_{fto}}\right] \tag{19}$$

Hence, the (rearward) shift in impact due to the retardation (equal to the difference in times of arrival) is equal to:

$$\Delta \underline{s} = \underline{V}_t \Delta t = R\underline{V}_t \left[\frac{1}{\underline{V}_{fta}} - \frac{1}{\underline{V}_{fto}}\right] \tag{20}$$

On average, the fragment originally ejected at an angle of:

$$\chi_o = \cos^{-1}\left[\frac{(\underline{V}_{fto} \bullet \underline{V}_t)}{|\underline{V}_{fto}||\underline{V}_t|}\right] \tag{21}$$

is now ejected with an average velocity $\underline{V}_{fta}$ at an average angle of:

$$\chi_a = \cos^{-1}\left[\frac{(\underline{V}_{fta} \bullet \underline{V}_t)}{|\underline{V}_{fta}||\underline{V}_t|}\right] \tag{22}$$

It must be noted that air drag becomes important when the warhead detonates long distances from the target, and hence retardation of fragments affects the flight trajectories and will cause a shift of impact points that may not be ignored, see Figure 9.

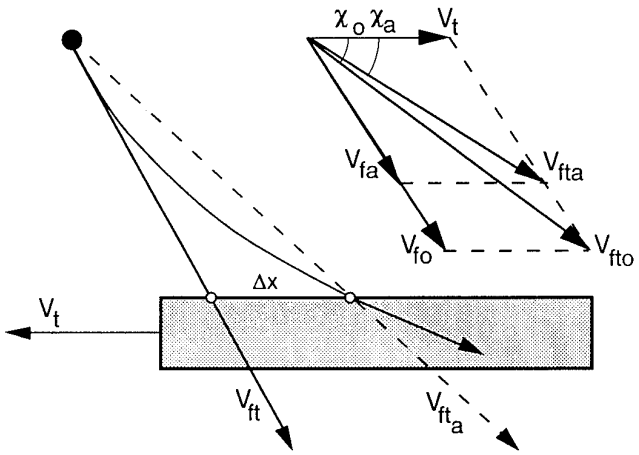

Figure 9 Effects of air drag on fragment trajectories

In MISDAC, it is simply assumed that for the velocities involved, a constant C_D may be taken, which is linearly interpolated for a given range of Mach numbers. The Mach number M is defined as:

$$M = \frac{V}{c_a} \tag{23}$$

where c_a is the speed of sound of the ambient air. For air, the speed of sound can be expressed as [8]:

$$c_a = \sqrt{\gamma \frac{R_a}{M_o} T} \tag{24}$$

where $\gamma = 1.4$ is the ratio of specific heats, $R_a = 8314.32$ Joule/K.kmol is the absolute gas constant, $M_o = 28.9644$ kg/kmol is the molecular weight of air and $T = 288.15$ K is the temperature. At sea level it yields: $c_a = 340.3$ m/s.
In [7] an equation is listed including the average shape numbers for a fragment and sphere as:

$$C_D = C_{D_{sphere}} + \left[\frac{S_n - S_{n_{sphere}}}{S_{n_{fragment}} - S_{n_{sphere}}}\right]\left\{C_{D_{fragment}} - C_{D_{sphere}}\right\} \tag{25}$$

where $S_{n_{sphere}}$=1.209 and $S_{n_{fragment}}$=1.856[1]. Table 1 lists some C_D values for a range of Mach numbers:

Table 1 *C_D values for a sphere and a (natural) fragment*

M →	0.0	0.7	1.1	5.0	9.0
$C_{D_{fragment}}$	1.06	1.09	1.40	1.20	1.12
$C_{D_{sphere}}$	0.47	0.57	1.00	0.91	0.91

The altitude of the weapon burst is included in the ambient density ρ_a, which is calculated according to the US standard atmosphere [8]. Given the velocity brackets, a look at Table 1 provides the necessary data for the drag coefficient to be used in equations (25), (16) and (17) to calculate the impact velocity at the target. To avoid unnecessary computations, a velocity deficit of 5 pct is taken as criterion, or referring to eqn. (17): F(R) = 0.95. Considering a general fragment with moderate velocity and drag coefficient, this results in the criterion for range, beyond which air drag calculations must be included as:

$$R_{drag} \geq 25 \frac{m^{1/3}}{\bar{S}_n} \quad \text{(m)} \qquad (26)$$

Hence, for a fragment of m=0.01 kg and $\bar{S}_n \approx 1.9$ this range becomes approximately 3 m, but for a large fragment (m=0.08 kg, $\bar{S}_n \approx 1.9$) this range becomes approximately 5.6 m.
Effects of gravity are excluded, since the trajectories considered are relatively short for gravity to become important.

3.5 Influence of fragment tumbling

To bring the tumbling of a fragment into account, the presented area of the fragment at the moment of impact (A_p) is assumed to vary slightly from its predetermined value between A_{min} and A_{max}.
A procedure to estimate the presented area for a beam-shaped fragment (at impact), viewed from a surrounding sphere with equally distributed viewpoints, resulting in a non-homogeneous area distribution is proposed in [9], see Figure 10.

1 In ref. [7] the US-based shape*factor* C [$ft^2 grain^{1/3}/lb$] is used, the conversion being: S_n= 3.25C.

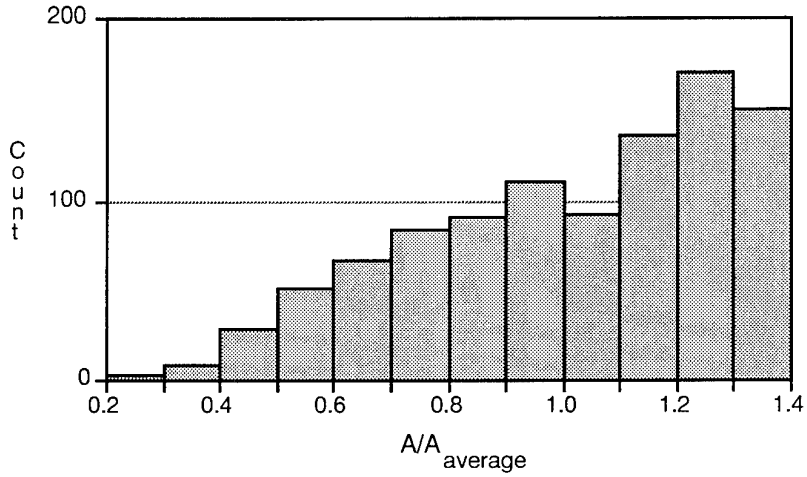

Figure 10 Presented area ratio histogram ($\bar{S}_n$=1.856 , based on 1000 samples)

The presented area at impact defines the impact shape number:

$$S_n = \frac{A_p}{Vol^{2/3}} \tag{27}$$

An example for three different shape numbers, i.e. for a sphere, a beam and a cube (with equal masses), is given in Figure 11.

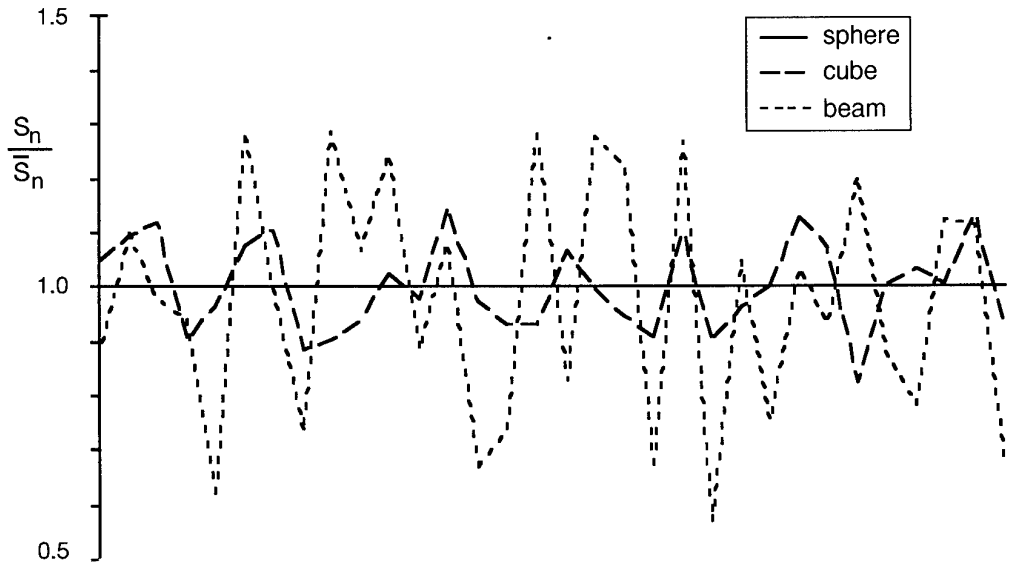

Figure 11 Effects of tumbling on impact shape number distribution

This approach demonstrates the possibility that from a class of fragments having an average shape number, which makes it impossible to penetrate a certain target plate, one or more impacting fragments will still be able to penetrate this plate due to the (randomly) reduced impact shape number.

In MISDAC, each "shot line" representing a fragment trajectory has a random shape number assigned to it corresponding with the random actual presented area at (first) impact. Each fragment is assumed to have a beam-like shape, which is expressed by the average shape number:

$$\bar{S}_n = \tfrac{1}{2}(ab)^{1/3}\left[1+\frac{1}{a}+\frac{1}{b}\right] \tag{28}$$

where a=L/t and b=w/t.
A procedure to estimate the values of a and b for an arbitrary (natural) fragment with a *given* shape number $\bar{S}_n$ is [9]:

$$\left.\begin{aligned} a &= 1+13.183\left(\bar{S}_n-1.5\right)\\ b &= 1+\ 4.700\left(\bar{S}_n-1.5\right)\end{aligned}\right\} \qquad (\bar{S}_n \geq 1.5) \tag{29}$$

The "optimal" values for a and b to match the beam with the given shape number can be found, using the "scaling" expressions, assuming a constant ratio of a/b:

$$a = a_o x \text{ and } b = b_o x \tag{30}$$

where a_o and b_o are the original constant values of a and b. A Newton-Raphson iteration is now used to find x, which estimates the roots of an equation according to the iterative relation:

$$x_{n+1} = x_n - \frac{f(x)}{f'(x)} \qquad n=1,.....m \text{ iterations} \tag{31}$$

where:

$$\left.\begin{aligned} f(x) &= \bar{S}_n - \tfrac{1}{2}(a_o b_o x^2)^{1/3}\left[1+\frac{1}{a_o x}+\frac{1}{b_o x}\right]\\ \frac{df(x)}{dx} &= -\tfrac{1}{6}(a_o b_o x^2)^{1/3}\left[\frac{2}{x}-\frac{1}{a_o x^2}-\frac{1}{b_o x^2}\right]\end{aligned}\right\} \tag{32}$$

This allows a quick assessment of the appropriate values for the equivalent beam-shaped fragment. It should be noted, that inserting the value $\bar{S}_n$ =1.5, which is the value for a cube where a/b=1, gives a trivial solution. Hence, the solutions found are valid for $\bar{S}_n \geq 1.5$.
For further penetration in the target, the value of the shape number is assumed constant for this trajectory since the effect of rotation velocity is neglected. If it assumed that the fragment rotates (tumbles) at ω=3000 rpm[1], then for a lateral velocity of V=1000 m/s, the distance for a complete rotation would be Δs=V/ω=20 m, which is much greater than the usual distances encountered in (aircraft) target (component) dimensions, apart from the maximum distance a fragment can penetrate into this target.

1 This value is considered extremely fast by ballistic experts at TNO-PML.

3.6 Impact and penetration

When the target is hit by the fragment (or projectile), the penetration capacity must be assessed. In general, for *steel* fragments hitting a target plate, the general THOR equation [10] is used, expressed by:

$$V_r = V - 10^{c1}\left[tA_p\right]^{c2} m^{c3} \sec\theta^{c4} V^{c5} \tag{33}$$

where V_r is the residual velocity, t is the target plate thickness[2], A_p is the presented area at impact, θ is the normal impact angle ($\sec\theta=1/\cos\theta$) and m and V are the mass and velocity of the fragment at impact. The THOR constants c_1 - c_5 are based upon experiments. Plotted on a log-log scale eqn. (33) provides linear terms, which can easily be used for fitting the constants with experimental data (e.g. multiple regression). The variables used and the shape of eqn. (33) does not have a physical background, except for their importance in ballistic experiments. It must be noted that the use of the constants are valid only within the limits of the experiments, and extrapolation to higher velocities, for example, will introduce errors. In fact, when the THOR equation is used for a higher velocity regime than the constants have been derived for, new experiments are required or erroneous results must be accepted.
The possibility of ricochet is included by limiting the impact angle $-70°\leq\theta\leq70°$ [11]. Shot lines impacting outside these boundaries are rejected (Figure 12).

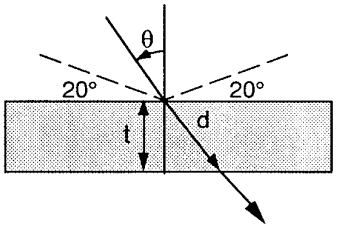

Figure 12 Impact situation at a plate

Using the impact shape number (eqn. 27), eqn. (33) can be rewritten as:

$$V_r = V - 10^{c1}\left[tS_n\rho_m^{-2/3}\right]^{c2} m^{\frac{2}{3}c2+c3} \sec\theta^{c4} V^{c5} \tag{34}$$

where ρ_m=7850 kg/m^3 is the density of steel, since THOR is valid for steel fragments. The maximum penetrable plate thickness - t_{max} - is found by setting V_r=0, which yields:

$$t_{max} = 10^{-c1/c2}\left[\frac{\rho_m^{2/3}}{S_n}\right] m^{-2/3-c3/c2} \sec\theta^{-c4/c2} V^{(1-c5)/c2} \tag{35}$$

This thickness is equal to the maximum distance (d_{max}) the fragment can penetrate into this target plate, while in general: d = tsecθ, where θ is the normal impact angle and d is the line-of-sight distance. From eqn. (35) it can be seen that t_{max} is inversely proportional with the shape number S_n. To illustrate the importance of the shape number, Figure 13 shows the effect of the

2 Not to be confused with penetration distance, or line-of-sight distance.

(impact) shape number on the maximum penetration capability for a number of impact velocities of a fragment mass of 25 gram impacting on an aluminium plate at normal obliquity.

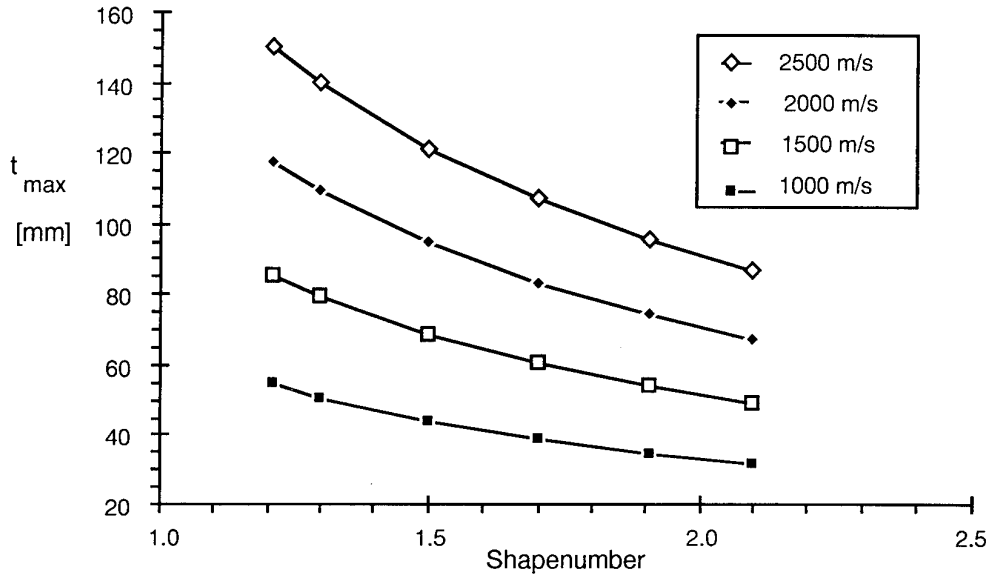

Figure 13 Effect of (impact) shape number on penetration capability

3.7 Blast effects

The effects of blast are hard to implement in a shot line oriented vulnerability code. A major variable in blast related analyses is the miss distance between the warhead burst point and the target. In MISDAC the blast vulnerable component is modelled as a line element, for which the miss distance can be easily derived. In parameter form the equation describing the position and orientation of the line $\underline{m}$ yields:

$$\underline{x} = \underline{M} + \lambda \underline{m} \tag{36}$$

where λ is a parameter, M is a fixed point on the line element (usually the centre position) and B is the warhead burst point (Figure 14).

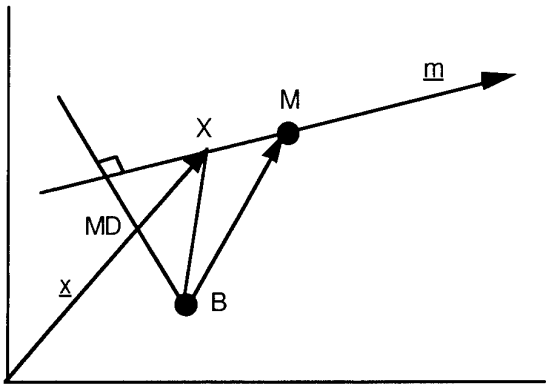

Figure 14 Definition of the miss distance

The line $\underline{BX} = \underline{X} - \underline{B}$ is normal to $\underline{m}$ if the scalar vector product equals zero, or:

$$(\underline{BX} \bullet \underline{m}) = 0 \tag{37}$$

or:

$$\left\{\left(\underbrace{\underline{M} + \lambda \underline{m}}_{\underline{X}} - \underline{B}\right) \bullet \underline{m}\right\} = 0 \tag{38}$$

from which λ can be solved as:

$$\lambda^* = \frac{\{(\underline{B} - \underline{M}) \bullet \underline{m}\}}{(\underline{m} \bullet \underline{m})} \tag{39}$$

The length of the vector $\underline{BX}^*$ is then equal to the miss distance MD to be found as:

$$MD = \left|\underline{M} + \lambda^* \underline{m} - \underline{B}\right| \tag{40}$$

The miss distance is a major variable which defines the encounter geometry (see also Figure 2). When a warhead detonation occurs, the blast wave generated is a spherical expanding wave, which can be characterised by its peak (side-on) overpressure p_s and positive duration t_p, see Figure 15. In general, the relation between peak overpressure and time is expressed by the modified Friedlander equation as:

$$p(t) = p_s\left[1 - \frac{t}{t_p}\right]\exp\left[-\beta\frac{t}{t_p}\right] \tag{41}$$

where ß is a slowly varying time factor, which is considered constant for this situation. A similar equation is used to describe the relation of the flow velocity or particle velocity as a function of time. For $t \geq t_p$, the pressure-time curve exhibits a negative phase, or suction phase, where the motion of (air) particles is reversed and is directed to the explosion source.

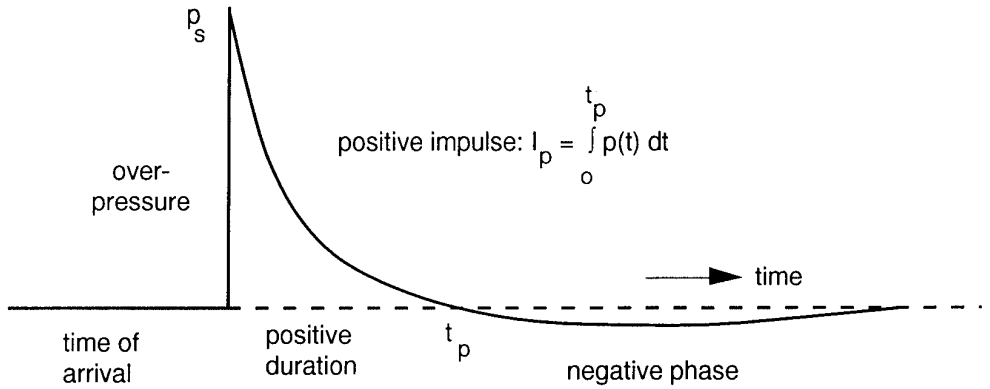

Figure 15 Blast wave characteristics

The motion of particles, denoted by their (flow) velocity u, will also create a dynamic pressure when their flow is distorted. If the flow would be isentropically brought to rest a dynamic pressure $q=\text{const.}\rho u^2$ is created, where ρ is the flow density. In a first approximation, the dynamic pressure originates from the one-dimensional Euler equation of motion [12]:

$$\frac{\partial u}{\partial t} + u\frac{\partial u}{\partial x} + \frac{1}{\rho}\frac{\partial p}{\partial x} = 0 \tag{42}$$

If the pressure wave would propagate without distortion and any decay, it can be written:

$$\frac{\partial u}{\partial t} \approx c\frac{\partial u}{\partial x} \tag{43}$$

where c is the wave speed (constant).
Inserting this term yields, assuming a constant density (incompressible):

$$\frac{\partial}{\partial x}(uc) + \frac{\partial}{\partial x}\left(\tfrac{1}{2}u^2\right) + \frac{\partial}{\partial x}\left(\frac{p}{\rho}\right) = 0 \tag{44}$$

which can be integrated to yield the equation:

$$\underbrace{p + \tfrac{1}{2}\rho u^2}_{\substack{\text{stagnation}\\ \text{pressure}\\ \text{(Bernoulli)}}} + \rho uc = \text{constant} \tag{45}$$

This equation differs substantially from the Bernoulli equation [12], which omits the term ρuc, but which is valid for a *steady* incompressible flow, i.e. $\partial u/\partial t = 0$. Basically, when the highly unsteady blast flow field is disturbed, the (unsteady) dynamic pressure - indicated by $\frac{1}{2}\rho u^2 + \rho uc$ - will be much larger than originally conceived from the Bernoulli equation. However, blast waves generally are not simple waves having a constant amplitude and speed. Table 2 lists a number of values for a spherical charge of TNT of 50 kg, which shows how fast a blast wave decays.

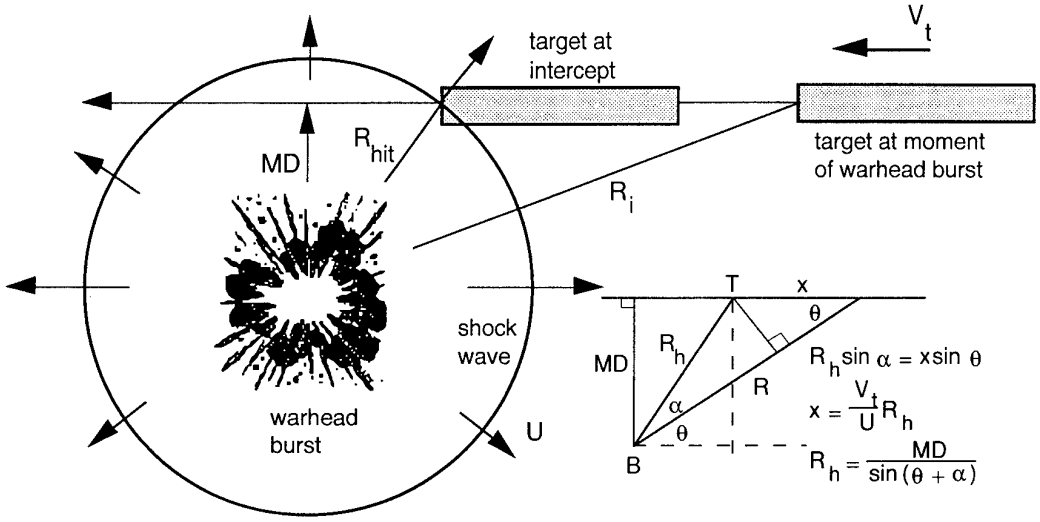

Figure 16 Effect of target velocity

The shock wave velocity can be approximated as:

$$U_s = a\left[\frac{R}{W^{1/3}}\right]^b \tag{47}$$

of which the constants are found using regression techniques. The *average* shock wave velocity can then be derived as:

$$\overline{U}_s = \frac{1}{Z - Z_c}\int_{Z_c}^{Z} U_s(x)dx \tag{48}$$

where $Z=R/W^{1/3}$ is the scaled range.
Using the expression of U_s, eqn. (47), the approximation yields for $0.053 \le Z \le 1.59$:

$$\overline{U}_s = \frac{2962}{Z - 0.052}\left\{Z^{0.3} - 0.412\right\} \quad (m/s) \tag{49}$$

The minimum range which should be observed is equal to the charge radius: $R_c = 0.053W^{1/3}$ (m), at which a "direct hit" or contact explosion occurs.
Based upon geometrical considerations (Figure 16) the distance at which the blast strikes the target can be found as [14]:

$$R_{hit} = \frac{R_i}{\sqrt{1 - \left[\frac{V_t MD}{\overline{U}.R_i}\right]^2} \pm \frac{V_t}{\overline{U}}\sqrt{1 - \left[\frac{MD}{R_i}\right]^2}} \tag{50}$$

where R_i is the initial distance at the moment of intercept. The "+" sign refers to an approaching target whereas the "-" sign refers to a target moving away. The average velocity $\overline{U}$ is based on the original range R_i. With respect to Figure 16, it can be shown that the sign is equivalent to the scalar vector product:

$$\text{sign} = -(\underline{BT} \bullet \underline{V_t}) \qquad (> 0 \text{ for an approaching target}). \tag{51}$$

As an example, consider a 50 kg charge of TNT detonating at an intercept range of 5 m from an approaching target flying at 300 m/s at a miss distance of 3 m. Then it follows that: $\bar{U}$ = 1935 m/s and $R_{hit} \approx$ 4.5 m, or a 10% reduction in range. This will give a distinct increase in peak overpressure, since the scaled range $R/W^{1/3}$, is reduced from 1.36 to 1.22 $m/kg^{1/3}$, respectively. The original peak static overpressure will increase from 430 to 600 kPa, which is an increment of almost 40%, because of the exponential behaviour of the overpressure-distance curve.
Apart from the virtual "closer" range, the blast wave will hit a moving target, which will have its impact on the dynamic reflection process. In general, shock wave reflection relations can be established for a stationary situation, but this changes dramatically when the target is moving. In addition, the blast loading duration on the target, defined by the time the shock wave needs to pass the target[1], will be reduced conversely (similar to the Doppler effect). Figure 17 illustrates these effects.
It is assumed that an ideal reflection takes place of a shock wave against an opposed moving wall with velocity -V, where M_A and M_B are the Mach numbers of the incident and reflected shock waves in regions 1 and 2, respectively (Figure 17).

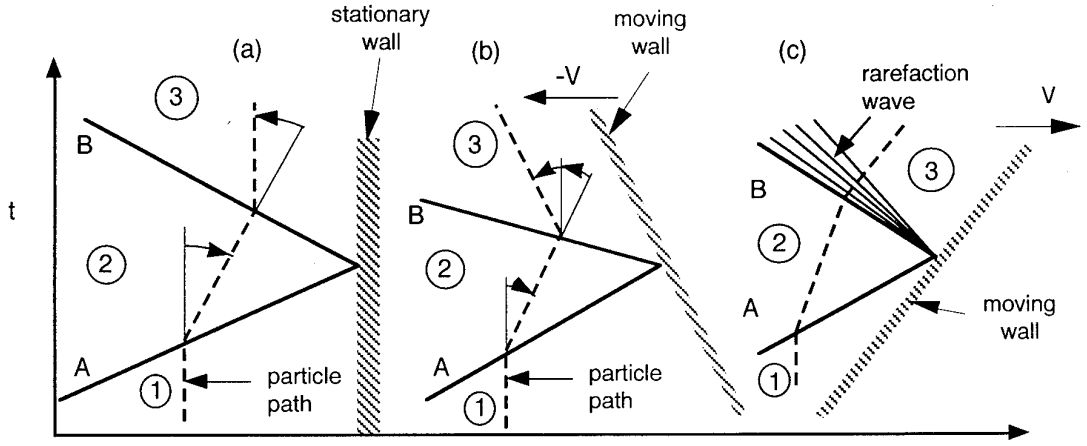

Figure 17 *Reflection against a stationary (a) and moving wall (b), (c)*
A - incident shock wave, B - reflected shock wave

A simple geometric consideration with respect to the boundary condition at the wall yields the reflection condition [12]:

$$u_3 - u_2 = -(u_2 - u_1) + V \tag{52}$$

where V is the wall velocity (positive to the right).
The Rankine-Hugoniot equations are used to express u_2, c_2 and u_3 in M_A and M_B:

$$\left.\begin{aligned} \frac{u_2 - u_1}{c_1} &= \frac{2}{\gamma+1}\left[M_A - \frac{1}{M_A}\right] \quad \text{right travelling wave} \\ \frac{u_3 - u_2}{c_2} &= \frac{-2}{\gamma+1}\left[M_B - \frac{1}{M_B}\right] \quad \text{left travelling wave} \end{aligned}\right\} \tag{53}$$

1 Called the diffraction loading.

Using the reflection condition, eqn. (52), M_B can then be solved from the resulting quadrature:

$$M_B^2 - M_B\left\{\frac{c_1}{c_2}\left[M_A - \frac{1}{M_A}\right] - \underbrace{\frac{(\gamma+1)}{2c_2}V}_{\text{dynamic reflection}}\right\} - 1 = 0 \tag{54}$$

from which the reflected pressure p_3 is calculated according to:

$$\frac{p_3}{p_2} = 1 + \frac{2\gamma}{\gamma+1}\left[M_B^2 - 1\right] \tag{55}$$

The reflected pressure p_3 can be put together in the reflection coefficient R_c, defined as:

$$R_c = \frac{p_3 - p_1}{p_2 - p_1} \tag{56}$$

Using the expressions for M_A and M_B, which yield solutions for p_2 and p_3, the reflection coefficient can be found as a function of the initial shock strength (or M_A). Omitting the details, Figure 18 shows the reflection coefficient for V=±300 m/s, which shows a dramatic difference with "normal" (i.e. V=0) reflection. When V is positive, an expansion may occur immediately behind the reflected shock wave, which is the case when the flow velocity u_2 is smaller than the wall speed. This phenomenon has been displayed in Figure 17 (c). In that case, the reflection overpressure decreases and even underpressure may develop.

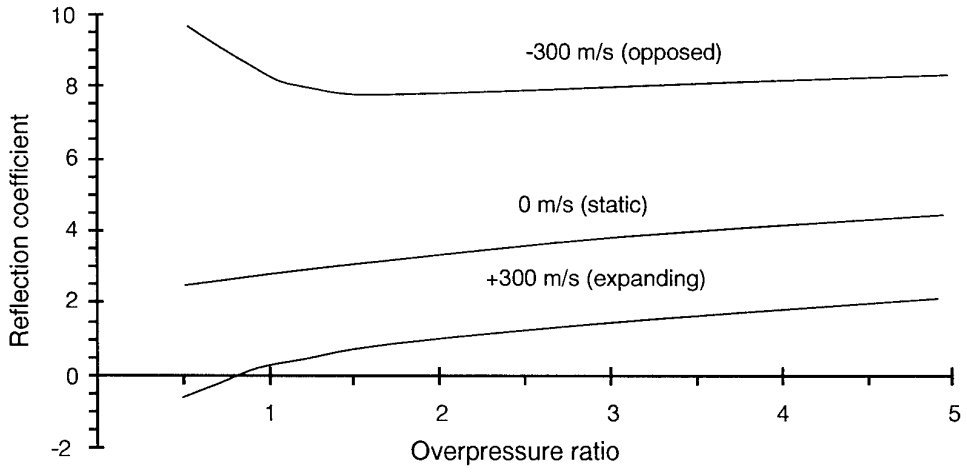

Figure 18 Dynamic reflection coefficient

It should be noted that R_c increases at low overpressure ratios (for an opposing wall), which is caused by the relatively large influence of V compared with the particle velocity. Conversely, this coefficient decreases for an expanding wall movement at low overpressure ratios. Obviously, when the wall speed is equal to the shock wave velocity itself, reflection does not occur at all. Another interesting feature is the diffraction impulse, which is controlled by the time the blast waves needs to "pass" the target. In general, this time can be expressed in terms of:

$$t_d = \frac{L}{U_s+V} \tag{57}$$

where L is an arbitrary dimension. The product of reflected pressure and diffraction period is then:

$$I_d = R_c t_d \tag{58}$$

which can be considered to represent the diffraction impulse. Figure 19 shows I_d as a function of the incident shock strength, and clearly shows that the net result will be a dramatic increase of impulse compared with the stationary target (V=0).

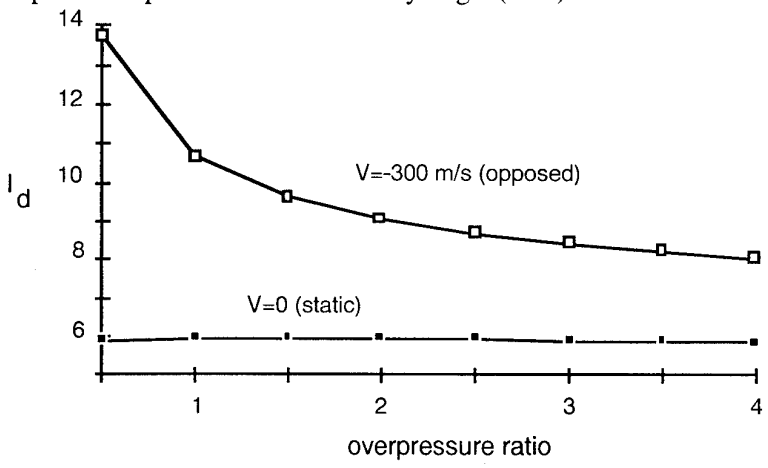

Figure 19 Reflection (diffraction) impulse

Despite the shorter duration (similar to the Doppler effect), the reflected pressure is much stronger leading to a significant increase in loading on the (opposed moving) target. Obviously, this effect will be reversed when the target moves away from the incoming shock wave, but this effect requires complex computations including interaction of rarefaction waves with shock waves, and is therefore omitted in this analysis.

MISDAC incorporates a blast kill routine (see paragraph 4.4) by assuming that the user provides blast-critical elements for the target. Each element is a line element, i.e. a cylindrical solid (with vulnerability code 2) with zero radius, so that only its orientation and length provide the essential information with respect to warhead burst point. For example, the vulnerability of the fuselage of a missile to blast is simply represented by a line in its centre, with a certain length. The code then determines the miss distance and the range of this element to the detonation point (which is assumed to occur in the centre of the warhead) and accounts for relative speeds to determine the range when hit by the blast. A structural analysis, however, is not performed, since this requires knowledge of blast loading histories (a problem on its own), structural layout (for example, a finite element analysis) and dynamic structural response analysis, which can usually be performed by advanced finite element codes. This combination is too cumbersome to apply in MISDAC, where use is made of simple analyses requiring characteristic properties. In general, when dealing with blast damage aspects, it is sufficient to employ global methods, such as the damage radius, which can be expressed by the Hopkinson scaled range $R/W^{1/3}$, irrespective of target orientation, size etc. Besides, it should be noted that blast damage is usually a secondary damage mechanism, since fragment damage dominates the overall damage capability of fragmenting

warheads. Paragraph 4.4 deals with the assumption put forward in the blast damage analysis such as used in MISDAC.

4 DAMAGE AND KILL CRITERIA

A major item in missile vulnerability assessment is the assignment of the appropriate damage criteria to the respective components considered. In MISDAC, four options exist to define specified damage criteria, viz.:

- Penetration damage (fragment/projectile)
  In general, this mechanism pertains to components having specific functions such as power transfer or to components that have not been described in detail, but in which certain, "processes" take place, such as electronics, gear box etc. For this kind of damage criterion, two options are:
  - complete penetration (perforation), e.g. holes in plates (fuel tanks) etc;
  - minimum penetration distance, e.g. plate thickness to be penetrated. For this mechanism, the t_{50} criterion is used (see later).

- Impact/Shock damage
  This mechanism occurs when a slug hits the component. The impact (kinetic) energy may cause shock damage, impact cratering and initiate other processes, such as shock initiation of explosives. For this mechanism, the critical kinetic energy criterion (E_{50}) is used.

- K(ill)-factor curves (direct component kill)

- Blast (shock wave) damage
  This mechanism applies when the warhead contains a large explosive charge (e.g. nuclear weapons, Fuel-Air explosives, large conventional weapons) whose primary effect (or in addition to fragment effects) is the blast wave striking the missile in flight. In general, the kill by blast is the structural kill. For this mechanism, the critical radius to the charge (R_{50}) is used as criterion.

Several options stem from the code TARVAC, but have been adapted for the purpose of missile damage assessments.
Basically, the probability of kill given a hit on a component (P_{kh}) by the threat is defined by:

$$P_{kh} = P_{dh}.P_{kd} \tag{59}$$

where:

P_{dh} probability of damage given a hit
P_{kd} probability of kill given damage

The first variable depicts the physical damage to a component, whereas the second variable more or less depicts the functional degradation of a component. Its combination, P_{kh}, does not reflect

the probability of kill of the *complete* missile, however, since this incorporates a systems kill in conjunction with residual flight capability to hit the target. Hence, eqn. (59) reflects the probability of kill for the internal components of a missile target (or any target), which will have further consequences for the missile's residual flight trajectory.
The probability of damage (of a component) is estimated given the damage mechanism (e.g. penetration) by a relation including the estimated critical value for that particular criterion, which is approximated by:

$$P_{dh} = \frac{x/x_{50}}{x/x_{50} + \exp\left[-\xi\left(x/x_{50} - 1\right)\right]} \tag{60}$$

where x_{50} is the estimated critical value indicating a 50% probability when the criterion (i.e. $x=x_{50}$) is met. This relationship is quite close to the normal cumulative probability distribution. The probability function accounts for the uncertainties in the assessment since the exact location of the hit and the direction the penetrator is going are averaged over the whole component, which virtually may have more than one vulnerable area. The variable ξ defines the deviation around x_{50}, or in fact the "accuracy" (or error) in the estimated critical value. Figure 20 shows the probability curve for a number of values of ξ.

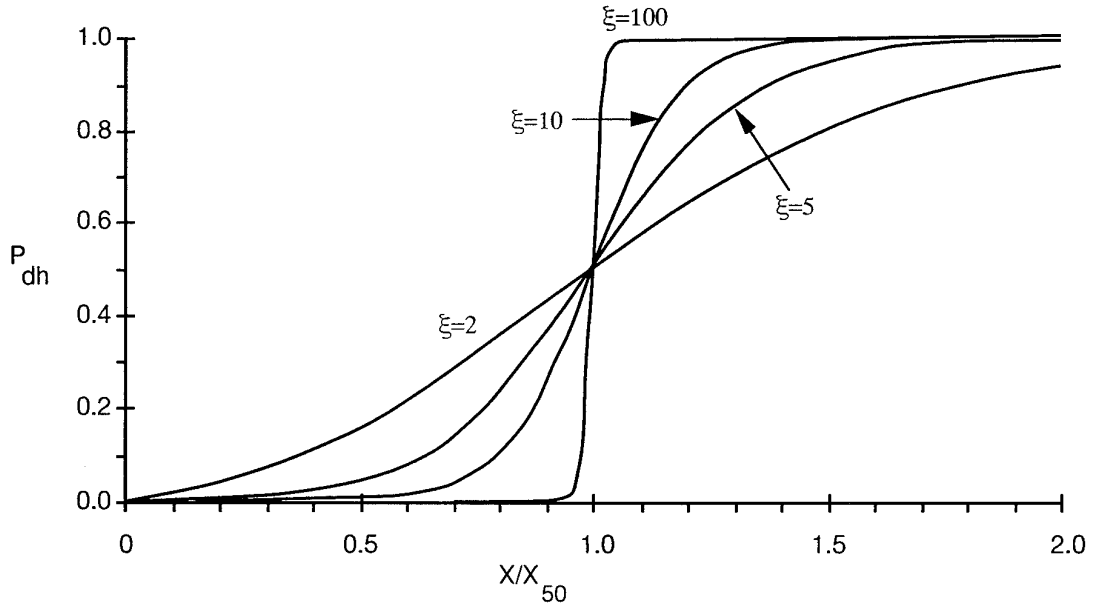

Figure 20 Damage probability curves for some ξ values

It can be shown that ξ can be related to the standard deviation (σ) of a normal distribution as [15]:

$$\xi = \frac{5/3 - \ln(\sigma + 1)}{\sigma} \tag{61}$$

4.1 Penetration damage criteria

For a penetrator, the penetration criterion is largely based on experimental data listed by the Thor penetration relation, valid for steel fragments, where the maximum penetration distance, see t_{max} from eqn. (35), is compared with the estimated critical value t_{50}.
The probability of kill given damage, P_{kd}, can be estimated utilising the Rayleigh (or Weibull (2,ß)) distribution [16]:

$$P_{kd} = 1 - \exp\left[-(y/ß)^2\right] \tag{62}$$

where $ß = y_{50}/\sqrt{\ln(2)}$ is the scale factor (with median y_{50}), or:

$$P_{kd} = 1 - \exp\left[-\ln(2)(y/y_{50})^2\right] = 1 - \left[\tfrac{1}{2}\right]^{(y/y50)^2} \tag{63}$$

which gives a 50% probability when $y=y_{50}$. This curve very much resembles the damage probability function when $\xi=2$ (equivalent with a normal distribution with $\sigma=0.6$). The probability function accounts for the uncertainties in the assessment of the (functional) kill of the component, which may depend on the location of the damage and/or the extent of damage inflicted. In eqn. (63) y/y_{50} is, for example, the effect of the penetration hole size (A/A_{50}) on the actual kill of the component given damage by a penetrator. For example, when A=0 while $P_{dh}=1$ then still $P_{kd}=0$, because a penetrator with an infinitely small penetration hole area cannot produce a kill. It may be noted that eqn. (60) may be used here also, but then the variable ξ must be specified, which introduces an extra variable.

4.2 Impact/Shock damage criteria

This mechanism is quite similar to the penetration process, where a fragment/projectile or a particle hits a component with a certain mass and velocity. Whether or not penetration or perforation is achieved, the impact kinetic energy may cause internal shock damage (mechanical accelerations), cratering or some other deformation. As the x_{50} criterion, the impact kinetic energy $E_{50} = 1/2mV^2$ is used, in addition to the probability equation (60). Similarly to the previous mechanism, the probability of kill given damage is assessed with the critical area A_{50} as the (y_{50}) criterion, since it is assumed that energy density (in fact E_{50}/A_{50}) is important in controlling the kill, see [20].

4.3 Direct kill criteria

A direct attempt to assess the kill of a component given a hit is the employment of the pre-determined vulnerability curves, indicated by a so-called K(ill)-factor [3]. The larger the value of K, the more vulnerable the component. At present, similar to TARVAC, MISDAC allows for up to nine levels, expressed by the variable $\log(mV^3)$ (Figure 21). The curves are categorised from "practically invulnerable" (K=1) to "highly vulnerable" (K=9) given a (single) hit. Selection of a specific value for a component's vulnerability should be preferably based on experimental data.

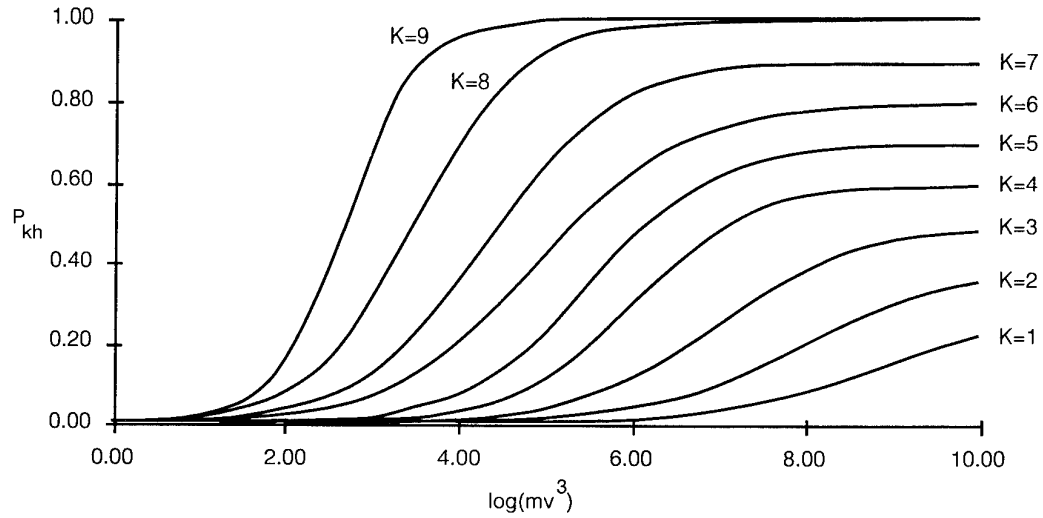

Figure 21 *Pre-determined kill probability curves (K-factor)*

In general, the kill probability given a hit using the K-factor is assumed by:

$$P_{kh_c} = \frac{a}{1 + \exp\left[-b\left(\frac{x}{c} - 1\right)\right]} \qquad (64)$$

and specific values for the constants a, b and c apply for various K-values, see Table 3.
This expression allows for the possibility that a component cannot be killed by a (single) fragment, e.g. such as may happen with a large electronic unit being hit by a relatively small fragment.

Table 3 *Values of vulnerability constants*

K	a	b	c
1	0.3	9.0	9.0
2	0.4	8.5	8.0
3	0.5	8.5	7.0
4	0.6	9.0	6.0
5	0.7	8.0	5.5
6	0.8	6.0	4.9
7	0.9	6.0	4.3
8	1.0	6.0	3.5
9	1.0	7.0	2.7

Some experimental data exist that nicely correspond to a specific K-value, but at the moment the basic principle(s) could not be verified, other than being the result(s) of extensive data analyses. One analysis indicates that the variable mV^3 - being rewritten as $V_m^{0.33}$ - corresponds quite well with associated Thor constants for V and m (1.0 and 0.333, respectively) for some materials used

in helicopter vulnerability studies, in which penetration criteria (t_{max}) based on Thor penetration relations were used.
In general, these curves may be applied for the kill assessment of complicated (and possibly large) components, where a single fragment causes damage, but not sufficient to produce a kill. Also, quick analyses can be performed when a target is composed of a large number of components (e.g. a ship).
The actual kill of a component given multiple hits by fragments can be assessed by the combination of their individual kill probabilities:

$$P_{kc} = 1 - \prod_{j=1}^{N} (1 - P_{kj}) \tag{65}$$

4.4 Blast damage criteria

As explained earlier, a structural analysis cannot be performed in a shotline oriented code such as MISDAC. However, it is sufficient to use global methods to account for structural response by employing the so-called blast damage radius, or critical blast radius. Basically, the target response is assumed to follow the P-I concept, where P stands for (maximum) applied load and I stands for (maximum) applied impulse. Any mechanical structure responds in a special manner to an applied load, but stays within two limiting realms, namely the quasi-static loading realm where the structural response depends only on P and the impulse loading realm where the structural response depends only on the impulse I. For any response between these boundaries, called the dynamic realm, the structural response depends both on P and I. It can then be shown [14],[17] that blast damage can be related to the main blast damaging parameters, viz. the range to the warhead (R) and the warhead size (W).
For (external) blast, the critical radius R_{crit} can be expressed by the Westine (R-W) vulnerability relation [17]:

$$R_{crit} = \frac{AW^{1/3}}{\left[1 + \frac{B^6}{W} + \frac{C^6}{W^2}\right]^{1/6}} \tag{66}$$

where A, B and C are component dependent constants[1] and W is the equivalent (spherical) free-air TNT charge weight. With the three constants given, it represents the entire range of loads of the blast wave on the structure. The equation covers the field from quasi-static (or pure pressure) loading (B=C=0) to combined pressure-impulse loading (C=0) up to purely impulsive loading (B=0). It must be noted that this equation may be regarded as a general vulnerability equation, since it implies target size, orientation and damage or failure mode, i.e. the extent and type of damage. In general, selecting specific values for the constants A, B and C implies one particular vulnerability curve in the R-W plane, but the target itself may be composed of several curves,

1 Similar to the Thor constants used in penetration analyses, the author suggests these constants to be called the Westine constants.

where the envelope determines its ultimate vulnerability. Also, no distinction is made between blast generated by internal or external explosions, or the effects of protection of a target by neighbouring components (shielding), which in fact obstructs the line-of-sight from the burst point to the target. However, incorporating these effects would require a dynamic target model, which is presently not at stake.
When dealing with high-velocity weapon-target interactions, such as in the case of a SAM warhead and sea skimming missiles, the (R,W) relation can be compensated for velocity effects [14], [18], [19]. Since a blast-critical component is modelled as a simple line element (i.e. cylinder with r=0), the critical radius R_{crit} is identical with the critical *miss distance* M_{50}. The probability of damage given a hit (P_{dh}) is estimated using an approximation similar to eqn. (60):

$$P_{dh} = 1 - \frac{x}{x + \exp\left[-\xi(x-1)\right]} \tag{67}$$

where $x = MD/M_{50}$ and where ξ may be selected as 2.0 (by default). Figure 22 shows the damage probability function for a number of ξ values.

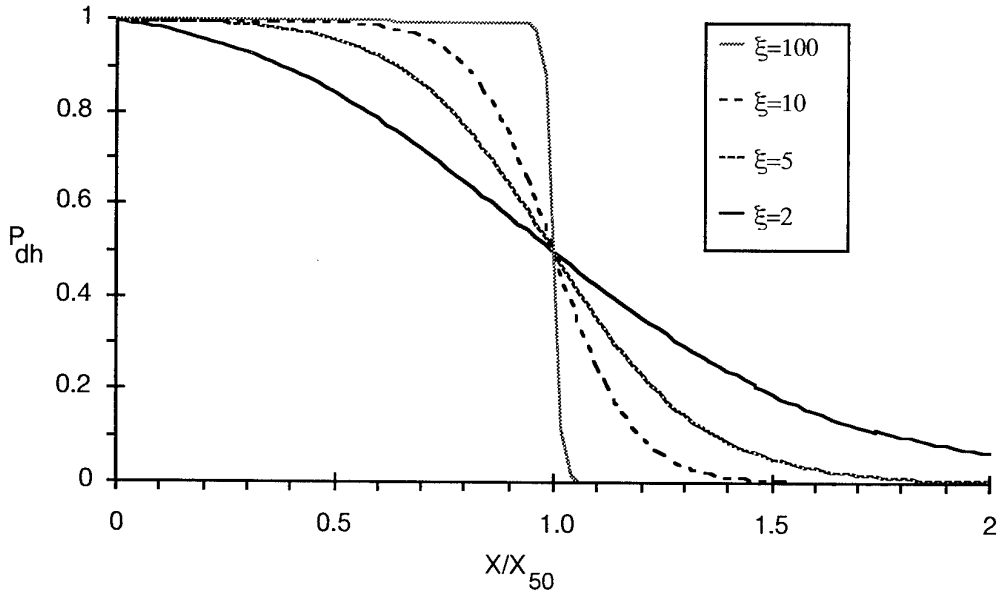

Figure 22 *(Blast) damage probability functions for some ξ values*

The probability of kill given damage can be derived taking the position of the burst point relative to the centre of the line element into account, which in fact accounts for the presented area. The probability of kill given damage, P_{kd}, is estimated utilising the Rayleigh probability density distribution:

$$P_{kd} = \exp\left[-\ln(2)\left(R/R_{50}\right)^2\right] = \left[\tfrac{1}{2}\right]^{\left(R/R_{50}\right)^2} \tag{68}$$

where $R_{50} = \sqrt{M_{50}^2 + (\frac{1}{2}L)^2}$, L is the length of the line element and R is the distance from the centre of the line element to the burst point. This approach assumes that the kill given damage by blast is related - in some way - to the way it interacts with the target, e.g. face-on or side-on with

respect to the general target dimensions. For example, a long rod or cylinder is quite sensitive to the exact location of the charge, while a sphere (or box) will be less sensitive. When dealing with very large planes, e.g. wing panels, it may be appropriate to construct this component with several line elements. However, it should be noted that *characteristic* features should be used. Hence, when dealing with wings, for example, the main wing spar(s) should be modelled since this structure carries the main load.

5 SYSTEMS DAMAGE EVALUATION

The final assessment of probability of kill of the target can be performed when it is known whether the (target) missile will hit its intended (ship) target. To this end, an estimate must be given of the damage inflicted to mission-sensitive systems, such as autopilot, aerodynamic control systems etc. Obviously, this is the most difficult part of the program, since an evaluation must be performed of the functional degradation of relevant systems, and its impact on continuing flight performance. This requires thorough knowledge of interior systems, and their functional relations with other systems on board. For example, when simulations indicate that the guidance unit will be hit several times by a number of fragments from a specific warhead, one should establish the effects it could impose on the flight computer output, i.e. steering signals to the rudder actuators. What will happen when signals are lost, e.g. caused by severance of the signalling cables to the rudder actuators? Also, in some instances some systems may become more important, and hence are more susceptible to failure. If, for instance, the warhead would be hammered such that a low order detonation (or even high order) is likely, then large pieces or debris of the missile will follow a ballistic trajectory and may inflict damage to the ship. To illustrate the difficulties, suppose that the sea skimming missile performs a dog-leg manoeuvre and is hit during the first leg, just before turning to the ship. If radar contact is present, but when controls fail and (supposedly) take a fixed position, then the missile would miss the ship entirely. If the missile is hit in the second leg it is already on course and may possibly hit the ship.
This part will be addressed in the next phase of the study, utilising a six-degrees-of-freedom (6-DOF) flight path simulation computer code, called FLIPSIM (Flight Path Simulation of Missiles) and assessment of systems damage and functional degradation.

6 DISCUSSION

The code MISDAC which has been described in this report, is a derivative of TARVAC, but includes many features of MISVAC. Basically, the geometrical target descriptions are the same, but weapons effects options have been reduced (no shaped charge effects, for example). However, blast damage and direct hit damage from intercepting air-defence missiles have been included, with the general assumption that blast damage does not prevail the overall damage assessment of missiles. The probability of kill given a hit has been assessed by two independent probability functions, viz. probability of damage given a hit and probability of kill given damage. This approach simplifies the input and reduces the number of variables compared with TARVAC while still retaining some "fuzzy" approach in the overall assessment.

7 CONCLUSIONS

A missile damage assessment code MISDAC has been derived from two formerly existing target vulnerability codes, i.e. the "standard" target vulnerability assessment code TARVAC and the derived missile vulnerability assessment code MISVAC.
The final kill probability assessment still has to be implemented using advanced six-degrees-of-freedom simulations to establish post-damage missile flight trajectories, which determine the overall missile kill probability given engagement by an air defence weapon. The new code assesses the damaging effects of fragments, projectiles and blast utilising probability functions and logical expressions. Fragmentation damage assessment has been improved by implementing random variation in impact shape (number), the variance being dependent on shape number (sphere $\rightarrow$ variance=0). Blast damage assessment has been simplified using blast-critical lines representing planes and/or components. An overall blast vulnerability equation employing three "Westine" constants determines the relation between critical distance and charge weight (R-W). Direct hit damage is also incorporated, which in general is assumed catastrophic for the target.

8 AUTHENTICATION

W. Haverdings
(author)

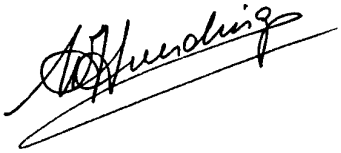

P.W. Doup
(Project leader)

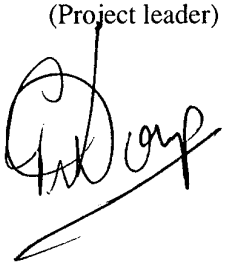

REFERENCES

1 Wolverton, M.A.
NATO AAW Missile Lethality Analysis
NWC TM 6606, December 1988, SECRET

2 Haverdings, W.
Effectiveness of the NATO AIM/RIM-7M Seasparrow missile warhead against various Anti-Surface-Ship-Missiles
Report PML 1992-3, January 1992, CONFIDENTIAL

3 Verheij, Z.C.
Method to determine the vulnerability of targets and the effects of projectiles (in Dutch), Part 1, 2, 3
PML 1986-22, 23, 24, 1986

4 Box, G.E.P.; Muller, M.E.
A note on the generation of random normal deviates
Annual Mathematical Statistics 29, 1958

5 Haverdings, W.
Dynamic projectile-target interactions
Memorandum PML-TNO, CoCo 1990-05-11-2, May 1990

6 Dehn, J.T.
Terminal effectiveness, vulnerability methodology and fragmentation warhead optimization. 1. A technical survey from a historical perspective
ARBRL-TR-02234, April 1980, AD-A085 021 (Unclass)

7 Doup, P.W.; Verheij, Z.C.
Influence of the shape of fragments on the results of vulnerability and lethality analyses
PML 1984-6, A79/KL/131, Assignment U 9103, 1984

8 Ruijgrok, G.J.J.
Data of the atmosphere (in Dutch)
Manual VTH-71, Technical University Delft
Department of Aerospace Engineering, January 1970

9 Galle, L.F.
A statistical method for the employment of fragment hit area in penetration equations or codes
Proc. 12th Int Symposium on Ballistics, San Antonio, 1990
Prins Maurits Laboratory TNO, Rijswijk, Netherlands, March 1990

10 Project Thor, Technical Report No. 47, April 1961
The resistance of various metallic materials to perforation by steel fragments; empirical relationships for fragment residual velocity and residual weight
Ballistic Analysis Laboratory, Institute for Co-operative Research
The Johns Hopkins University

11 NIAG Very Short Range Air Defence (VSRAD)
Methodology for Lethality and Vulnerability Assessment
NIAG SG33/T1/82005/2, October 1990, NATO Secret

12 Shapiro, A.H.
The dynamics and thermodynamics of compresssible fluid flow, Vol 2
The Ronald Press Company, New York, 1954

13 Swisdak, M.M.
Explosion effects and properties. Part 1: Explosion effects in air
NSWC/WOL/TR 75-116, 6 October 1975, AD-A018 544

14 Haverdings, W.
A simple blast model for target vulnerability assessments
PML 1990-IN68, December 1990

15 Smit, C.S.
Notes on the kill probability curve used in TARVAC (in Dutch)
Unpublished notes, 9 February 1990, also in memo: CoCo 1990-05-08-1

16 Law, A.M.; Kelton, W.D.
Simulation modelling and analysis
McGraw-Hill, Inc., 2nd edition, 1991, ISBN 0-07-036698-5

17 Westine, P.S.
R-W plane analysis for vulnerability of targets to air blast
The Shock and Vibration Bulletin 42, Part 5, January 1972

18 Campbel Fred, Chief of Staff
Elements of Terminal Ballistics
Part One: Introduction, Kill Mechanisms, and Vulnerability
Headquarters US Army Materiel Command, Washington 25, DC
AMCP 706-160 (SECRET), 30 November 1962
Degraded unclassified 16 March 1976

19 Sewell, R.G.S.
Blast overview and near-field effects
NWC Technical Memorandum 3754, February 79, AD-A088239

20 Angelucci, S.B; Biseröd, J.F.; Gondet, J.F.; Groessler, P; Held, M; Hughes, D.P.; Kantner, H.; Lursat, D.; Mariani, S.; Minion, R.J.; Nicholson, J.; Price, A.R.; Rentzsch, A.R.; Thompson, A.; Zech, G von.; White, A.J.
Target Neutralization - Final Report
NIAG SG 9 - Part III - Book 7, T9/08/R, Volume 7 to Part III to NIAG (77) D/1, AC/141(PG/17)D/6, NATO Confidential

REPORT DOCUMENTATION PAGE
(MOD NL)

1. DEFENSE REPORT NUMBER (MOD-NL)	2. RECIPIENT'S ACCESSION NUMBER	3. PERFORMING ORGANIZATION REPORT NUMBER
TD94-0474		PML1994-A33
4. PROJECT/TASK/WORKUNIT NO.	5. CONTRACT NUMBER	6. REPORT DATE
232492170	A92/KM/407	September 1994
7. NUMBER OF PAGES (excl. RDP, distr. list)	8. NUMBER OF REFERENCES	9. TYPE OF REPORT AND DATES COVERED
43	20	Final

10. TITLE AND SUBTITLE

General description of the Missile Systems Damage Assessment Code (MISDAC)

11. AUTHOR

W. Haverdings

12. PERFORMING ORGANIZATION NAME(S) AND ADDRESS(ES)

TNO Prins Maurits Laboratory, Lange Kleiweg 137,
P.O. Box 45, 2280 AA Rijswijk, The Netherlands

13. SPONSORING AGENCY NAME(S) AND ADDRESS(ES)

KM/DMKM/WCS/HGW,
P.O. Box 20702, 2500 ES The Hague

14. SUPPLEMENTARY NOTES

The classification designation ONGERUBRICEERD is equivalent to: UNCLASSIFIED

15. ABSTRACT (MAXIMUM 200 WORDS (1044 BYTE))

A computer code MISDAC (Missile Systems Damage Assessment Code) has been developed by which the damaging effects of an exploding warhead or hitting projectiles against an antiship missile can be assessed. The code is largely based on two already existing computer codes, but has been substantially changed to make it also applicable against future threats for a ship. The damaging effects include structural (or gross) damage due to blast effects and damage due to a direct hit by the intercepting missile.

MISDAC allows the damage assessment of any missile target and is not restricted to certain types of targets, such as envisioned in a former code (MISVAC), where only three generic anti-ship missiles could be analysed.

The outcome of MISDAC is suited to establish the final assessment of kill of the attacking antiship missiles, where a kill means that the missile or its debris will miss the ship. Many factors are influential, such as the distance to the ship when the missile is damaged (the target-range-to-go), the type of manoeuvre it is performing (dog-leg, weave etc.), the flying altitude and the damage inflicted to the missile's flight-essential systems. To this end, use is made of advanced six-degrees-of-freedom (6-DOF) calculations to determine the post-damage trajectory of the missile, which is performed by the code FLIPSIM (Flight Path Simulation of Missiles). With these simulations, the actual size of the ship can be included, making the final probability of kill even dependent on the type of ship considered.

16. DESCRIPTORS		IDENTIFIERS
Computer program	Anti-ship missiles	
Missiles	Target Vulnerability	
Projectiles	Kill probability	
Warheads	Blast effects	
Damage		

17A. SECURITY CLASSIFICATION (OF REPORT)	17B. SECURITY CLASSIFICATION (OF PAGE)	17C. SECURITY CLASSIFICATION (OF ABSTRACT)
ONGERUBRICEERD	ONGERUBRICEERD	ONGERUBRICEERD

18. DISTRIBUTION AVAILABILITY STATEMENT	17D. SECURITY CLASSIFICATION (OF TITLES)
Unlimited Distribution	ONGERUBRICEERD

Distributielijst*

1*	DWOO
2*	HWO-KL
3*	HWO-KLu
4	HWO-KM
5	KM/DMKMWCS/HGW, KLTZ Ir. M.A. van Maanen
6/8	TDCK
9	Bureau TNO-Defensieonderzoek
10	TNO-FEL, Ir. P.F. Ruizendaal
11	Der Wehrtechnische Studienbeauftragte der BundesWeher, Dipl. Ing. J.R. Höflein
12*	Lid Instituuts Advies Raad PML Prof. B. Scarlett, M.Sc.
13*	Lid Instituuts Advies Raad PML Prof. ir. M.A.W. Scheffelaar
14*	Lid Instituuts Advies Raad PML Prof. ir. K.F. Wakker
15	TNO-PML, Directeur; daarna reserve
16	TNO-PML, Directeur Programma; daarna reserve
17	TNO-PML, Divisie Wapens en Platforms, Dr. R.R. IJselstein (Divisiehoofd)
18	TNO-PML, Groep WapenEffectiviteit, Ir. Z.C. Verheij (Groepshoofd)
19	TNO-PML, Groep WapenEffectiviteit, Ir. W. Haverdings (Auteur)
20	TNO-PML, Groep WapenEffectiviteit, Ir. P.W. Doup (Projectleider)
21	TNO-PML, Groep Ballistiek, Dr. H.J. Reitsma (Groepshoofd)
22	TNO-PML, Divisie M&E, Groep Explosiepreventie en Bescherming Dr. Ir. J. Weerheijm (Groepshoofd)
23	TNO-PML, Documentatie
24	TNO-PML, Archief
25/28	TNO-PML, reserve

---

* De met een asterisk (*) gemerkte instanties/personen ontvangen uitsluitend de titelpagina, het managementuittreksel, de documentatiepagina en de distributielijst van het rapport.